BIOMACROMOLECULES

ARTICLE

pubs.acs.org/Biomac

This document is shared for only research purposes and cannot be distributed without the permission of the authors and the publisher.
Please visit WWW.BECERGROUP.SEMS.QMUL.AC.UK/PUBLICATIONS.HTML to get more info on our research interests!!!

Functionalized, Biocompatible Coating for Superparamagnetic Nanoparticles by Controlled Polymerization of a Thioglycosidic Monomer

Krzysztof Babiuch,[†] Ralf Wyrwa,[‡] Kerstin Wagner,[‡] Thomas Seemann,[‡] Stephanie Hoeppener,[†,§] C. Remzi Becer,[†,⊥] Ralf Linke,[∥] Michael Gottschaldt,[†,§] Jürgen Weisser,[‡] Matthias Schnabelrauch,[‡,§] and Ulrich S. Schubert*[,†,§]

[†]Laboratory of Organic and Macromolecular Chemistry (IOMC) and Jena Center for Soft Matter (JCSM), Friedrich-Schiller University Jena, Humboldtstr. 10, 07743 Jena, Germany

[‡]Biomaterials Department, INNOVENT e.V., Prüssingstr. 27b, 07745 Jena, Germany

[§]Dutch Polymer Institute (DPI), John F. Kennedylaan 2, 5612 AB Eindhoven, The Netherlands

[⊥]Department of Chemistry, University of Warwick, Library Road, CV4 7AL Coventry, United Kingdom

[∥]Surface Engineering Department, INNOVENT e.V., Prüssingstr. 27b, 07745 Jena, Germany

Supporting Information

ABSTRACT: It is demonstrated that water-soluble, glucosylated poly(pentafluorostyrene) derivatives revealed favorable coating material properties for magnetic iron oxide nanoparticles. To prepare the coating material in high reproducibility and purity as well as in sufficient amounts, a new route of synthesis is established. The preparation and characterization of the glucosylated, tetrafluorostyryl monomer, by thiol-*para*-fluorine "click" reaction, and its polymerization, via nitroxide-mediated radical process, is presented in detail. In addition, the coating material and the resulting particle properties are investigated by means of XPS, DLS, TGA, TEM, and cryo-TEM as well as flow cytometry. The glycopolymer acts as an appropriate stabilizing agent for the superparamagnetic nanoparticles by the formation of an approximately 10 nm thick shell, as shown by the XPS analysis. Furthermore, the application of FITC-labeled glycopolymer yielded fluorescent, superparamagnetic nanoparticles, which can be used for monitoring cell−carbohydrate interactions, because these particles show no cytotoxicity toward 3T3 fibroblasts.

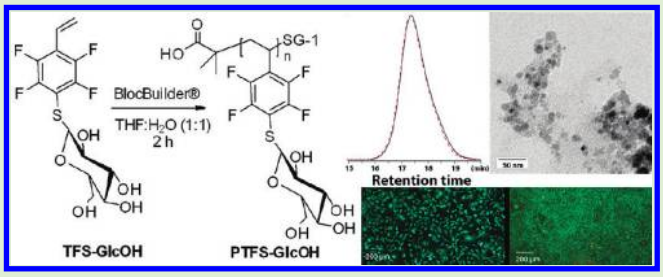

INTRODUCTION

Superparamagnetic nanoparticles based on iron oxide are of increasing importance in the fields of bioanalytics and medicine. The advantage in using iron oxide as magnetic material is its known low cytotoxicity and high biocompatibility. As a consequence, magnetic nanoparticles can potentially be used in a wide range of biomedical applications. Some examples include magnetic resonance imaging (MRI), cell separation, magnetic drug targeting, and hyperthermia cancer treatment as well as magnetofection.[1−6] The advances in the field of magnetic nanoparticle design for medical purposes have been reviewed recently.[7] Shell materials for magnetic nanoparticles used in these applications include polysaccharides, for example, dextran or derivatives thereof, in particular, carboxymethylated dextran, poly(ethyleneimine), poly(*N*-isopropyl-acrylamide), poly(ethyleneglycol), or vinyl alcohol-based polymers among others.[8−12] The polymeric materials that are suitable for biomedical usage and used for coating and stabilization of iron oxide particles have to fulfill similar requirements, that is, water solubility and no or only little cytotoxicity. In general, the shell of the polymer prevents agglomeration by steric effects as well as electrostatic repulsion, enabling the stabilization of individual magnetic cores. These biocompatible, polymer-coated nanoparticles exhibit sufficient stability in diluted aqueous solution and allow the modification of physical and chemical properties by varying the structure of the polymer. In addition, functionalities, such as OH-, NH-, or carboxylic groups, allow further introduction of functional moieties like drugs and bioactive ligands, for example, carbohydrates, proteins, or dyes, enabling drug targeting with directed cell interaction or usage in bioanalytical applications.[13−16] The main drawback for a broad medical use of magnetic nanoparticles is their insufficient long-term stability. Although technical ferrofluids possess extraordinary stability, the coating materials and their synthesis strategy cannot be applied to iron oxide nanoparticles in aqueous

Received: November 6, 2010
Revised: December 17, 2010
Published: January 21, 2011

 © 2011 American Chemical Society

solution since they are not soluble in water. Examples of frequently used coating materials of technical ferrofluids are fatty acids and polymers, for example, poly(styrene).[17,18] To combine the advantages of polymers used in technical ferrofluids (stability) with the requirements of medically applicable magnetic nanoparticles, it is necessary to develop water-soluble, noncytotoxic, polymeric nanoparticle coating materials. In principle, glycopolymers, that is, synthetic polymers carrying pendant sugar moieties, fulfill the above-mentioned requirements. Furthermore, these polymers have found a wide range of applications in clinical diagnostics, as targeted drug delivery systems, for affinity separations, bioassays, and biocapture analysis.[19−22] Their therapeutic applications have been thoroughly reviewed.[23] In spite of their biomedical significance, only very few synthetic glycopolymers have been applied as coatings of magnetic beads.[24−26] To the best of our knowledge, only one single report of poly(vinylbenzyl-*O*-β-D-galacto-pyranosyl-D-gluconamide)-coated iron oxide nanoparticles as a liver-targeting MRI contrast agent exists.[27] Recently, glycopolymers based on poly(pentafluorostyrene) were synthesized using a versatile "click" approach.[28,29] They consist of a carboxylic acid terminated chain and thioglucose substituted, fluorinated phenyl rings. These linear, saccharide functionalized polymers show a suitable water solubility mediated by the sugar moieties. The additional carboxylic function could permit the electrostatic interaction with the iron oxide surface as known principle of attachment.[2] For reproducible preparation of ferrofluids, structurally well-defined glycopolymers are required. For this purpose, a new route of synthesis was established. In contrast to our previous work, where the glycopolymers were obtained by postpolymerization modification of preformed polymeric backbones, herein the sugar-modified polymers were obtained by a direct polymerization of glucosylated monomers. Coupling of acetylated β-D-thioglucopyranose via a nucleophilic substitution of para-fluorine of pentafluorostyrene and subsequent deacetylation with sodium methoxide provided a glycomonomer with an overall yield of 84%. Its optimized, nitroxide-mediated, radical polymerization gave a glycopolymer with high monomer conversion (70%) and low polydispersity index (PDI < 1.2). This glycopolymer fulfilled all the requirements for preparing stabilized, water dispersible, magnetic nanoparticles because it was able to withstand the harsh conditions used in the coating procedure. Furthermore, for the planned medical use the cytotoxicity of this type of polymer was investigated. No cytotoxic effects were found. Herein, the synthesis of a new glycosylated tetrafluorostyrene monomer, its controlled radical polymerization, labeling and application as fluorescent, biocompatible coating material for superparamagnetic nanoparticles based on iron oxide as well as their detailed characterization are reported.

EXPERIMENTAL SECTION

Materials. 2,3,4,6-Tetra-*O*-acetyl-1-thio-β-D-glucopyranose was synthesized as previously reported.[30] Triethylamine (TEA; for synthesis, ≥99%), ferrous chloride tetrahydrate (p.a.), 25% ammonia solution (p.a.), and potassium permanganate (0.1 N, Titrisol) were purchased from Merck, *N*,*N*-dimethylformamide (DMF; ≥99.5%), *N*,*N*-dimethylacetamide (DMA), sodium thiosulfate solution (0.1 M, Fixanal), and anthrone (p.a., ACS reagent) from Fluka, fluorescein isothiocyanate isomer I (FITC, ≥90%; HPLC) from Sigma, methanol (anhydrous, 99.8%) from Aldrich, and ferric chloride hexahydrate (p.a., ACS reagent), and 37% hydrochloric acid (HCl; p.a., ACS reagent) from Roth. Sodium methanolate was purchased from Fluka and stored under argon prior to use. All other chemicals were used as received, unless otherwise noted.

Characterization. ^{1}H and ^{13}C NMR spectra were recorded on a Bruker Avance 300 MHz spectrometer and the ^{19}F NMR spectra on a Bruker Avance 200 MHz spectrometer in deuterated DMF. The chemical shifts were calibrated with respect to DMF residual peaks. Size exclusion chromatography (SEC) was measured on an Agilent Technologies 1200 Series gel permeation chromatography system equipped with a G131A isocratic pump, a G1329A autosampler, a G1362A refractive index detector, and both a PSS Gram 30 and a PSS Gram 1000 columns in series. LiCl solution (2.1%) in DMA was used as eluent at 1 mL·min^{-1} flow rate at a column oven temperature of 40 °C. The reported number average molar masses were calculated according to poly(styrene) standards. For homogenization of the particles a Sonopuls UW2200 (Bandelin, Germany) device was used. Dynamic light scattering measurements (DLS) were performed on a Zetasizer device from Malvern Instruments (Worcestershire, U.K.). The magnetic behavior was measured with a vibrating sample magnetometer (MicroMagTM, Princeton Measurement Corp., US, B_{max} = 1.6 T). X-ray photoelectron spectroscopy (XPS) was measured with a Theta Probe system (Thermo VG Scientific) equipped with monochromatic X-ray Al Kα source (1486.68 eV) using a spot diameter of 400 μm (100 W) and the analyzer in CAE mode with a pass energy of 150 eV for survey spectra and 75 eV for elemental region spectra. The spectra were collected with an angle of 53° to the surface normal and an angle acceptance of ±30° and charging compensation by low energy electrons was applied. The CasaXPS v2.14 software was used for XPS data processing. Electron binding energies (BE) were corrected by adjusting the low energy component of the C1s emission to 284.8 eV. Relative sensitivity factors based on the Scofield cross sections were used for quantification assuming a homogeneous distribution of the components in the probed sample volume. Peak positions and contributions of different chemical states were determined by fit processing. Thermogravimetric analyses were performed on a Netzsch TG 209 F1 Iris with 10 °C·min^{-1} heating rates from room temperature up to 900 °C, with a two-minute isothermal step at 450 °C, under nitrogen flow. Flow cytometry was measured on a Beckmann Coulter Cytomics FC-500 equipped with Uniphase Argon ion laser, 488 nm, 20 mW output. Transmission electron microscopy (TEM) as well as cryo-TEM images were recorded using a Technai G2 Sphera (FEI) TEM with an acceleration voltage of 200 kV. Fluorescence of the cells was observed using an Axiovert 25 microscope (Zeiss AG, Jena, Germany) with filter sets 44 and 14. Photomicrographs were recorded using a CCD fluorescence imager MP 5000 (Intas, Göttingen, Germany). Imaging was supported by the Image-Pro Plus software (Media Cybernetics, Silver Spring, MD).

Cell Culture. The 3T3 fibroblasts (from the DSMZ German Collection of Microorganisms and Cell Cultures, Braunschweig, Germany) were cultured in DMEM supplemented with 10% fetal calf serum, 50 U·mL^{-1} penicillin, and 50 μg·mL^{-1} streptomycin (all components from Biochrom, Berlin, Germany), under 5% CO_2 atmosphere at 37 °C.

Synthesis of the Glycomonomer

a. Synthesis of 4-(2,3,4,6-Tetra-O-acetyl-1-thio-β-D-glucopyranosido)-2,3,5,6-tetrafluorostyrene (TFS-GlcAc). 2,3,4,6-Tetra-*O*-acetyl-1-thio-β-D-glucopyranose (3.30 g, 9.06 mmol) was dissolved in 90 mL of dry DMF in a round-bottom flask and cooled in an iced water bath. Pentafluorostyrene (1.25 mL, 9.20 mmol) was added dropwise to the stirred solution. Subsequently, TEA (2.55 mL, 18.30 mmol) was dropped into the reaction mixture. The reaction was continued for 3 h at room temperature until complete disappearance of the starting sugar, monitored by TLC in hexane/ethyl acetate (1:1). The solvent and the small excess of pentafluorostyrene were removed in a rotary evaporator, and the crude product was purified by column chromatography (hexane/ethyl acetate (1:1)) on silica gel. The solvent mixture was evaporated and the product was dried under vacuum to give 4.39 g (90% yield) of a white powder. ^{1}H NMR (300 MHz, DMF-d_7, δ): 6.81 (1H, dd, $^3J_{1',2'}$ = 17.9 Hz, $^3J_{1',3'}$ = 11.9 Hz, CH-vinyl), 6.18 (1H, dd, $^2J_{2',3'}$ = 75.8 Hz,

CH_2-vinyl), 5.93 (1H, dd, CH_2-vinyl), 5.40 (1H, t, $^3J_{4,3}$ = 9.4 Hz, H-4), 5.35 (1H, d, $^3J_{1,2}$ = 10.4 Hz, H-1β), 5.06 (1H, t, $^3J_{3,2}$ = 9.6 Hz, H-3), 4.99 (1H, t, H-2), 4.23 (1H, dd, $^2J_{6',6}$ = 12.8 Hz, $^3J_{6',5}$ = 6.3 Hz, H-6′), 4.14−4.04 (2H, m, H-6, H-5), 2.12, 2.04, 2.01, 2.00 ppm (12H, 4s, CH_3-acetyl). ^{13}C NMR (300 MHz, DMF-d_7, δ): 171.0, 170.8, 170.6, 170.5 (CO-acetyl), 150.5−150.2 (m, C−F), 147.3−147.0 (m, C−F), 144.0−143.7 (m, C−F), 126.3 (t, $^4J_{C,F}$ = 30.2 Hz, CH_2-vinyl), 123.2 (CH-vinyl), 119.5 (t, $^2J_{C,F}$ = 55.7 Hz, C−S), 110.0 (t, $^2J_{C,F}$ = 84.6 Hz, C−C), 85.5 (C1), 76.4 (C5), 74.4 (C4), 71.8 (C2), 69.3 (C3), 63.1 (C6), 21.0, 20.9, 20.8 ppm (CH_3-acetyl). ^{19}F NMR (200 MHz, DMF-d_7, δ): −134.2 (2F, m), −144.9 ppm (2F, m).

b. Synthesis of 4-(1-Thio-β-D-glucopyranosido)-2,3,5,6-tetrafluorostyrene (TFS-GlcOH). 3.00 g (5.57 mmol) of TFS-GlcAc was added to 200 mL of dry methanol to give a milky suspension. Under vigorous stirring, 11.15 mL of a 2 M solution of sodium methanolate was added dropwise to the reaction mixture. After 15 min, a clear solution was obtained. The reaction was continued until complete disappearance of the starting material (1 h), monitored by TLC (silica gel, ethyl acetate/hexane (1:1) and ethyl acetate/methanol (3:2) to confirm complete deprotection). Subsequently, the mixture was neutralized with Dowex 50WX8−200 H^+-loaded resin, filtered and dried under vacuum. TFS-GlcOH was obtained as a white powder (1.92 g, 93% yield). ^{1}H NMR (300 MHz, DMF-d_7, δ): 6.77 (1H, dd, $^3J_{1',2'}$ = 17.9 Hz, $^3J_{1',3'}$ = 11.9 Hz, CH-vinyl), 6.12 (1H, dd, $^2J_{2',3'}$ = 78.3 Hz, CH_2-vinyl), 5.86 (1H, dd, CH_2-vinyl), 5.71 (1H, s, OH), 5.36 (1H, bs, OH), 5.17 (1H, bs, OH), 4.93 (1H, d, $^3J_{1,2}$ = 9.5 Hz, H-1), 4.48 (1H, t, $^3J_{OH,CH3}$ = 5.8 Hz, OH), 3.79−3.68 (1H, m, H-6), 3.54 (broad signal, H_2O and H-6′), 3.43 (1H, t, $^3J_{4,3}$ = 8.3 Hz, H-4), 3.36−3.23 ppm (3H, m, H-2, H-3, H-5). ^{13}C NMR (300 MHz, DMF-d_7, δ): 150.0 (m, C−F), 146.4 (m, C−F), 143.8 (m, C−F), 125.3 (t, $^4J_{C,F}$ = 30.2 Hz, CH_2-vinyl), 123.3 (CH-vinyl), 117.6 (t, $^2J_{C,F}$ = 56.7 Hz, C−S), 112.0 (t, $^2J_{C,F}$ = 85.6 Hz, C−C), 86.8 (C1), 82.9 (C5), 79.8 (C4), 75.9 (C2), 71.6 (C3), 62.7 ppm (C6). ^{19}F NMR (200 MHz, DMF-d_7, δ): −136.0 (2F, m), −145.9 ppm (2F, m). HRMS (ESI, m/z): Calcd for $C_{14}H_{14}F_4O_5SNa$ $[M + Na]^+$, 393.0766; found, 393.0390. Anal. Calcd for $C_{14}H_{14}F_4O_5S\cdot 2H_2O$: C, 41.38; H, 4.46; S, 7.89. Found: C, 41.54; H, 4.02; S, 7.91.

c. Polymerization of TFSGlcOH. Glucosylated monomer (500 mg, 1.35 mmol), BlocBuilder (from Arkema, 10.3 mg, 0.027 mmol), tetrahydrofuran (5 mL), and water (5 mL) were added in a 20 mL pressure-resistant vial. The mixture was saturated with argon while stirring for 1 h. The vial was sealed and placed into a preheated oil bath (110 °C). The reaction was continued for 2 h. Afterward, the reaction vessel was cooled with tap water and the solution was concentrated in the rotary evaporator prior to precipitation in cold ethanol. The isolated white powder of PTFS-GlcOH (350 mg) was dried under vacuum. The conversion (70%) and the degree of polymerization (DP) of 30 were estimated from ^{1}H NMR spectra of the mixture before and after polymerization, using THF as the internal standard. ^{1}H NMR (300 MHz, DMF-d_7, δ): 5.62 (m, OH), 5.30 (m, OH), 5.13 (m, OH), 4.77 (m, H-1), 4.30 (m, OH), 3.90−3.14 (broad signal, H_2O, CH_2-ethanol and H-2, 3, 4, 5, 6, 6′), 2.36−1.88 (broad signal, CH_2-backbone), 1.39−0.8 ppm (broad signal, CH_3-initiator and CH_3-ethanol). ^{13}C NMR (300 MHz, DMF-d_7, δ): 149.5−142.0 (m, C−F), 123.0−120.0 (m, C−F), 111.8 (m, C−F), 87.0 (C1), 81.4 (C5), 78.5 (C4), 74.8 (C2), 70.2 (C3), 61.5 (C6), 56.9 (CH_2-ethanol), 39.6−28.9 (DMF and backbone carbons), 18.2 ppm (CH_3-ethanol). ^{19}F NMR (200 MHz, DMF-d_7, δ): −132.1 to −136.5 (m), −141.4 to −146.4 ppm (m).

d. FITC-Labeling of PTFS-GlcOH. In an oven-dried, round-bottom flask, the glycopolymer (451.0 mg, 0.04 mmol) and FITC (7.6 mg, 0.02 mmol) were weighed in and dried for 1 h under vacuum. DMF (10 mL) was added, and the sealed mixture was stirred for 24 h. The reaction was quenched and the polymer precipitated by dropping the solution into ethanol. The precipitated polymer was centrifuged and washed with ethanol until complete disappearance of fluorescence in the supernatant (six times, TLC monitoring).

Synthesis of Iron Oxide Nanoparticles. Superparamagnetic iron oxide nanoparticles consisting of magnetite and maghemite, with an average core diameter of 10 nm were prepared as previously described.[31] Briefly, aqueous mixtures of iron salts with a molar ratio of 1/2 ($FeCl_2$/$FeCl_3$) were coprecipitated by adding an excess of 25% aqueous ammonia solution. The particles were separated magnetically, washed repeatedly with distilled water, and the pH value was adjusted to 1−2 with HCl.

Particle Coating. A total of 250 mg of the PTFS-GlcOH glycopolymer, dissolved in 30 mL of distilled water, was added to a freshly prepared ferrofluid at 50 °C. Subsequently, the mixture was stirred at 50 °C for 20 min. A first particle fraction was separated magnetically and discarded to get rid of larger, uncoated particles. After adjustment of the pH value of the supernatant to 5, a second fraction was isolated magnetically and washed repeatedly with distilled water. Finally, the core−shell particles were resuspended in water and homogenized by ultrasonic treatment. The coating with FITC-labeled glycopolymer was carried out analogously.

Characterization of the Nanoparticles. The iron(II) and iron(III) contents were determined after dissolution in HCl (37%) by conventional titration with $KMnO_4$ and $Na_2S_2O_3$, respectively. The characterization data of the magnetic behavior (specific saturation magnetization, δ_s, coercive field strength, H_c, and relative saturation remanence, δ_r/δ_s) of the nanoparticles (powder from lyophilization as well as ferrofluid) was obtained from the curve of magnetization, recorded with a vibrating sample magnetometer. Dynamic light scattering (DLS) was used to study the size (hydrodynamic diameter, h_d), zeta potential (ζ), and particle polydispersity index (PDI_p). Samples were strongly diluted in double distilled water (5 μL of the ferrofluid in 4 mL of water for the determination of size and 50 μL in 4 mL of water for the determination of zeta potential). The size distribution was reported by intensity.

a. Sugar Titration. The glucose unit, bound to the poly(tetrafluorostyrene) backbone, was used for the determination of the shell material content in an adapted procedure of Dreywood, Gutierrez-Gallego, and Scott.[32−34] In brief, the method is based on the conversion of polysaccharides into monosaccharides through acid hydrolysis, and the conversion of monosaccharide-derived furfurals into an UV/vis-absorbing complex with the tricyclic aromatic hydrocarbon anthrone. The peak maximum of the anthrone-complex was determined at a wavelength of λ = 625 nm. The sample was prepared by dissolving the nanoparticles in HCl (37%) followed by the described procedure. Based on a calibration curve, the amount of shell material could be determined.

b. TEM and Cryo-TEM Measurements. Dry samples were prepared by blotting the 10-fold diluted solution onto a carbon coated TEM grid (Electron Microscopy Science) placed on a filter paper. Samples for cryo-TEM were prepared using a FEI Vitrobot system. A total of 3 μL of the sample solution was transferred onto a Quantifoil (R2/2) grid, and blotting was performed at 3 mm and 3.5 s of blotting time. Samples were rapidly transferred into liquid ethane and stored in liquid nitrogen until the measurements were performed using a Gatan cryo holder.

Investigation of Cytotoxicity. The biocompatibility of the magnetic nanoparticles was investigated in a live/dead assay using 3T3 cells and fluorescent dyes: fluorescein diacetate (FDA, labeling live cells) and ethidium bromide (EtBr, labeling the nuclei of dead cells).[35,36] The 3T3 cells were inoculated at 25000 cells·cm^{-2} into a 48-well tissue culture plate (Greiner Bio-One, Frickenhausen, Germany) and cultivated for 6 h at 37 °C under a 5% CO_2 atmosphere. The culture medium (0.5 mL) was supplemented with 1, 5, and 25 μL of the polymer-coated nanoparticles to give the final concentrations of 0.2, 1, and 5% (v/v), respectively. The tests were performed in duplicate after 1 and 4 days with addition of 0.5 mL of the nutrient medium after two days. The live/dead staining followed the standard protocol. After 1 and 4 days, the culture medium was withdrawn and the cells were covered with 0.1 mL of PBS (to avoid the drying of the cells) and with 0.1 mL of 2-fold

Scheme 1. Schematic Representation of the Synthesis of the Glycopolymer

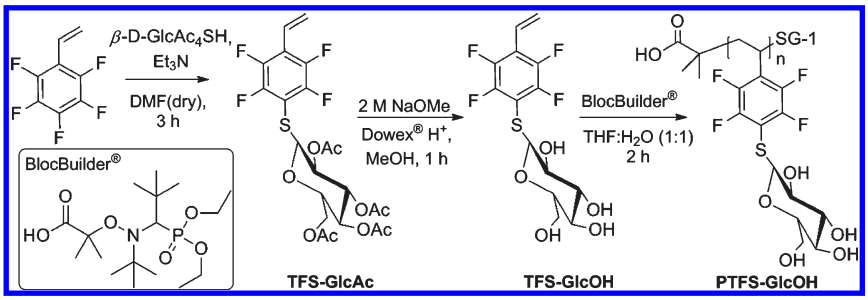

concentrated staining solution realizing the final concentrations of 15 $\mu g \cdot mL^{-1}$ FDA and 4 $\mu g \cdot mL^{-1}$ EtBr. The observation of the red and green fluorescence started after 1 min by fluorescence microscopy. The total number of cells and the percentage of living cells were calculated from the micrographs by counting the orange-fluorescent nuclei of the dead cells and the green-fluorescent living cells.

RESULTS AND DISCUSSION

Glycopolymer Synthesis. To evaluate pentafluorostyrene-based glycopolymers as potential coating material for superparamagnetic iron oxide nanoparticles, well-defined polymers of high purity and large quantity are required. The methods of glycopolymer synthesis have been the subject of many reviews.[22,37−43] Basically, sugar-modified polymers can be obtained by two approaches, namely, the polymerization of glycosylated monomers or the grafting of sugar moieties onto a preformed polymeric backbone. Herein, the first method was employed since the reactants, pentafluorostyrene and thioglucose tetraacetate, are commercially available, and the applied polymerization technique, the nitroxide-mediated radical polymerization (NMP), yields products with low polydispersity indices (PDIs) and good conversions for styryl-based monomers.[44−46] Furthermore, NMP does not require any toxic catalyst or heavy metal salt to mediate the reaction, which represents a major disadvantage for most of the other polymerization methods and was already previously applied to obtain poly(styrene)-based glycopolymers.[47−55] The procedure for the synthesis of the glycomonomer and the subsequent polymerization is illustrated in Scheme 1.

i. Thiol-para-fluorine "Click" Reaction. Significant contributions have concentrated on the glycomonomer synthesis because they are usually not commercially available.[40,56] The synthesis of the sugar-bearing monomers most often requires multistep procedures.[41,42] The thiol-*para*-fluorine reaction was previously reported as an efficient route to functionalize poly(pentafluorostyrene) with acetylated, thiosugar moieties.[28,29] Furthermore, the reactivity of the *para*-fluorine on the pentafluorophenyl group is significantly enhanced if soft primary nucleophiles are used.[57,58] The potential, versatility, and effectiveness of thiol-halogen nucleophilic reactions were recently summarized in an excellent review.[59] Moreover, this method results in the formation of materials with *S*-glycosidic bound sugar residues, which are, unlike *O*- and *N*-glycosidic bonds, stable against enzymatic degradation.[60−62] Herein, 2,3,4,6-tetra-*O*-acetyl-1-thio-β-D-glucopyranose (GlcAcSH) was reacted with pentafluorostyrene (PFS) in the presence of triethylamine in dry dimethylformamide (DMF). The reaction was carried out at a nearly equimolar ratio of GlcAcSH to PFS. A slight excess (1 mol %) of pentafluorostyrene was used to ensure the full conversion of the carbohydrate. The synthesis proceeded

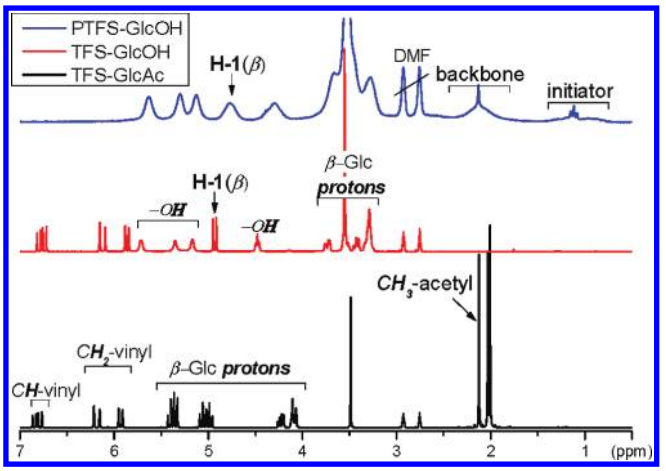

Figure 1. ^{1}H NMR (DMF-d_7, 300 MHz) spectra of synthesized monomers and the glycopolymer.

quantitatively, and after 3 h, GlcAcSH was completely converted to TFS-GlcAc, as shown by TLC monitoring. The acetylated monomer was purified from triethylammonium fluoride by column chromatography and dried to obtain a white powder in high yield (90%). ^{1}H, ^{13}C, ^{19}F, and HSQC-DEPT NMR spectroscopy confirmed the structure and the purity of TFS-GlcAc (Figure 1 and Supporting Information).

The proton spectrum exhibits only the required peaks for the acetylated β-glucose moiety and the vinyl group. In the ^{19}F spectrum, only the signals from *ortho*- and *meta*-fluorines are visible (Figure 2).

ii. Carbohydrate Deprotection. The final glycomonomer was obtained by applying the standard Zemplén procedure for sugar deprotection as described in the Experimental Section. The purity and structure of TFS-GlcOH was determined by ^{1}H, ^{13}C, ^{19}F, and HSQC-DEPT NMR spectroscopy as well as electrospray ionization mass spectrometry (ESI-MS) and elemental analysis. The complete deprotection is confirmed by the disappearance of the methyl proton signals of the acetyl groups in the ^{1}H NMR spectrum and the appearance of four peaks corresponding to the hydroxyl groups of the deacetylated β-D-glucose substituent (Figure 1).

iii. Polymerization of TFS-Glucose. For the polymerization of the glucosylated tetrafluorostyryl monomer via nitroxide-mediated controlled, radical polymerization, a β-phosphonylated alkoxyamine initiator (BlocBuilder from Arkema, Scheme 1) was used. The synthesis was carried out in a pressurized vial in a THF/H_2O (1:1) mixture, with a monomer to initiator ratio of 50, at 110 °C for 2 h. After cooling, the solution was concentrated and precipitated

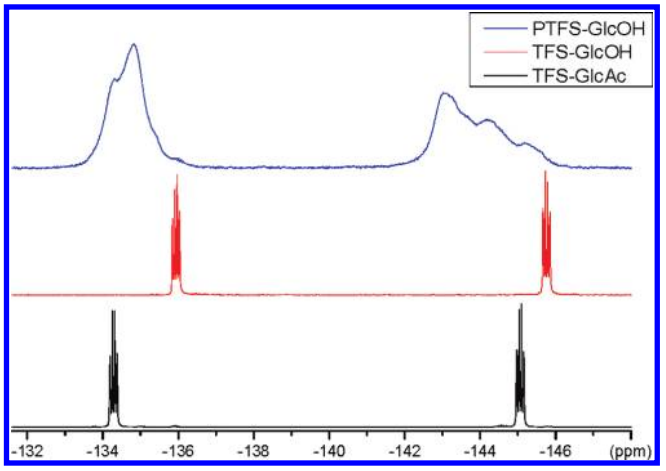

Figure 2. ^{19}F NMR (DMF-d_7, 300 MHz) spectra of synthesized monomers and the glycopolymer.

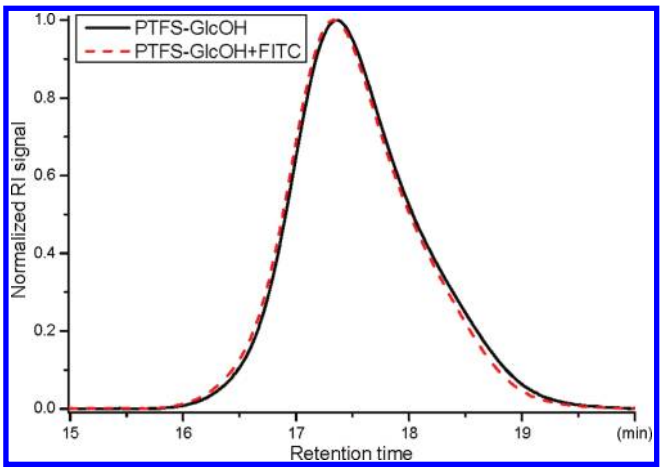

Figure 3. SEC traces of the synthesized glycopolymers in *N*,*N*-dimethylacetamide with lithium chloride (2.1 g·L^{-1}) as eluent.

in cold ethanol. The isolated white powder of PTFS-GlcOH (350 mg, 70% conversion, DP = 30) was characterized by ^{1}H, ^{13}C, ^{19}F NMR, and HSQC-DEPT spectroscopic methods as well as by size exclusion chromatography (SEC). The proton spectrum (Figure 1) of the glycopolymer shows the signals of the β-D-glucose moieties, the polymeric backbone, and the initiator. The ^{19}F NMR spectrum (Figure 2) exhibits two broad signals corresponding to the *ortho*- (−132.1 to −136.5 ppm) and *meta*-fluorines (−141.4 to −146.4 ppm) of the tetrafluorostyryl units. The broadening of the signals and the local maxima are due to the different tacticities of the glycopolymer. The SEC trace (Figure 3) of the obtained polymer shows a narrow, monomodal distribution.

The molar mass of 24000 g·mol^{-1} and the PDI value (1.16) were calculated according to poly(styrene) standards (from PSS). From the SEC analysis results it can be concluded that the polymerization was carried out in a controlled fashion, thus a well-defined glycopolymer was obtained.

iv. Fluorescence Labeling of the Glycopolymer. For labeling of PTFS-GlcOH, the glycopolymer (0.04 mmol) and fluorescein isothiocyanate (FITC, 0.02 mmol) were vacuum-dried and dissolved in 10 mL of DMF in a round-bottom flask. After stirring for 24 h at room temperature, the polymer was precipitated and purified by repeated washing in ethanol and centrifugation. A total of 350 mg of yellowish powder were obtained. SEC analysis of the fluorescent polymer (Figure 3) shows a slight increase, from 24000 to 24300 g·mol^{-1} of the molar mass. The low PDI value of 1.16 was maintained for the labeled glycopolymer, signifying no coupling reactions of the polymeric backbone or its decomposition.

Synthesis and Characterization of the Glycopolymer-Coated Superparamagnetic Iron Oxide Nanoparticles. The superparamagnetic particles were produced by coprecipitation of iron chlorides with 25% aqueous ammonia as reported in the literature.[31] Coating of the obtained particles with both labeled and nonlabeled glycopolymer was accomplished in aqueous, acidic solutions (pH = 1−2) at 50 °C within 20 min. The shell−core particles were magnetically separated and thoroughly washed with distilled water. To confirm the success of the coating procedure and to estimate the quantity of the glycopolymer attached to the particle, they were investigated by means of dynamic light scattering (DLS), transmission electron microscopy (TEM), X-ray photoelectron spectroscopy (XPS), thermogravimetric analysis (TGA), flow cytometry (FC), and iron as well as sugar titrations. Furthermore, their magnetization behavior was examined.

i. Particle Characterization by DLS. For the investigation of the particles via DLS, the obtained ferrofluids were highly diluted in double-distilled water (5 μL of the ferrofluid in 4 mL of water for the determination of size and 50 μL in 4 mL of water for the zeta potential investigation). For this study, suspensions of naked and coated with unlabeled PTFS-GlcOH particles were used. The summary of the obtained results can be found in Table 1. The noncoated nanoparticles exhibit an average hydrodynamic diameter value of 140 nm. After the coating procedure, this value increased to an average of 329 nm indicating successful binding of the glycopolymer. Furthermore, the change of the zeta potential (ζ) of the particles from the positive value of 28 mV to negative (−2.3 mV) provides a confirmation of the presence of the glycopolymer on the iron oxide core.

ii. Titration Analyses of the Glycopolymer-Coated Nanoparticles. The obtained glycopolymer-coated and uncoated particles were chemically analyzed in view of the overall iron content as well as the iron(II) to iron(III) ratio by titration experiments, following the standard procedures.[63] The selective determination of iron(II) and iron(III) by titration with $KMnO_4$ and $Na_2S_2O_3$, respectively, yielded in 3.4 mg·mL^{-1} of iron(II) and 20.0 mg·mL^{-1} of iron(III) for the suspension of the noncoated particles and 1.4 mg·mL^{-1} of iron(II) and 9.8 mg·mL^{-1} of iron(III) for the one containing the coated particles (Table 1). To obtain further information of the amount of coating on the nanoparticles, the amount of glucose units, bound to the poly(tetrafluorostyrene) backbone, was quantified by the anthrone assay as described in the Experimental Section. Based on a calibration curve, the amount of shell material could be determined. The content of 7.5 mg·mL^{-1} of glucose was obtained for the nanoparticle suspension, confirming the presence of the glycopolymeric coating material.

iii. Analysis of the Magnetization Behavior. The magnetization behavior of noncoated and coated particles was analyzed using a vibrating sample magnetometer. The fluids as well as the lyophilized powders were investigated. The results of the analysis, obtained from the curve of magnetization, are summarized in Table 1. Both samples revealed superparamagnetism. Furthermore, the magnetization behavior indirectly confirms the presence of the glycopolymeric material since the specific saturation

Table 1. Characterization Data of the Naked and Glycopolymer-Coated Particles[a]

sample	H_c [kA·m^{-1}]	δ_s [Am^2·kg^{-1}]	$\delta_r \cdot \delta_s^{-1}$	Fe(II) content [mg·mL^{-1}]	Fe(III) content [mg·mL^{-1}]	h_d (PDI$_p$) [nm]	ζ [mV]
powder							
naked	0.7	66.0	0.02				
coated	0.3	32.2	0.01				
suspension							
naked	0.8	1.8	0.03	3.4	20.0	140 (0.22)	28
coated	0.7	0.4	0.03	1.4	9.8	329 (0.24)	−2.3

[a] H_c, coercive field strength; δ_s, specific saturation magnetization; $\delta_r \cdot \delta_s^{-1}$, relative saturation remanence; h_d, hydrodynamic diameter; ζ, zeta potential.

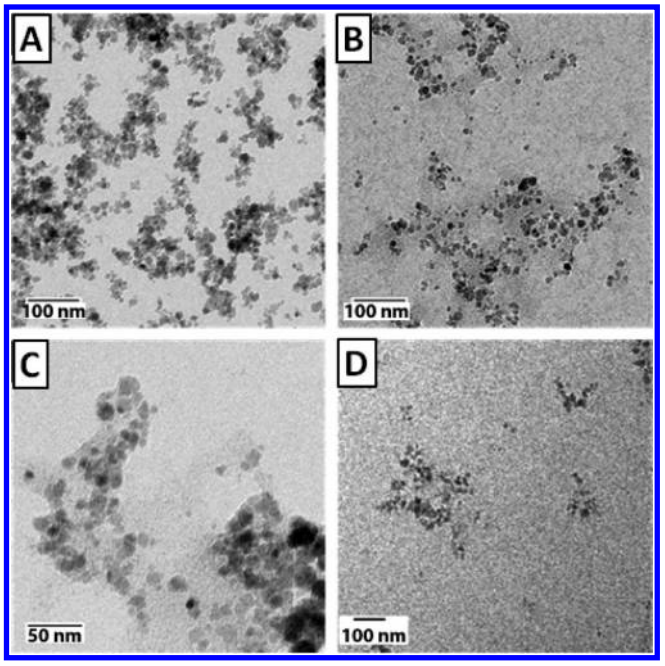

Figure 4. TEM micrographs of the naked (A) and glycopolymer-coated (B, C) iron oxide nanoparticles and a cryo-TEM image of the coated particles (D).

magnetization (δ_s) is significantly lower for the modified particles due to the layer of the coating material, consistently to the results previously obtained for cyclodextrin- and carboxymethyl dextrane-functionalized iron oxide particles.[64,65] Moreover, the relative saturation remanence (δ_r/δ_s) is distinctly lower for the coated particles, signifying that a stable aqueous suspension of superparamagnetic particles was obtained.[66] The above-mentioned properties allow a highly efficient magnetic manipulation when used in bioseparation or as a drug carrier under relatively low external magnetic field. In addition, these particles are possible candidates for application as magnetic resonance contrast agents in cellular and molecular imaging.[67]

v. Particle Characterization by TEM. To investigate differences in shape and architecture of the glycopolymer-coated particles, the structure of the obtained core−shell, superparamagnetic particles was investigated. TEM investigations (Figure 4) were used to determine the diameter of the individual iron nanoparticles, which revealed a typical size of less than 15 nm, both for noncoated and coated particles. Compared to the typical diameter of the particles measured by DLS, the individual iron particles appear to be much smaller, indicating that the DLS measurements provide the hydrodynamic diameter of particle agglomerates. The nonhomogenous distribution of the particles on the TEM grid (Figure 4A) might support this assumption. However, also drying artifacts will influence the distribution of the particles. In contrast to the noncoated particles, the presence of a polymer network is observed in case of coated nanoparticle assemblies (Figure 4B and 4C). The overall diameter of the interlinked assemblies is observed to be a few hundred nanometers, which is in agreement with the trend to increased particle sizes measured by DLS for the coated nanoparticles. This system was further investigated by means of cryo-TEM investigations (Figure 3D), which permit the imaging of a solution-like state of the nanoparticles. The coated nanoparticles also reveal a state of association here, with assemblies of an average diameter of 100−300 nm, which is in good correlation with DLS as well as dry TEM measurements.

v. Particle Characterization by XPS. X-ray photoelectron spectroscopy is a potent tool to characterize surface coatings. Not only does it provide information about the elemental composition, it also gives data about the chemical states present in the analyzed sample as well as the coating thickness.[11] Therefore, the naked and the glycopolymer-coated iron oxide particles have been investigated by XPS (Figure 5 and Table 2).

In the survey spectrum of the uncoated iron oxide nanoparticles (Figure 5A), mainly O and Fe are found as expected. Additionally, a small amount of carbon is detected. The C signal is attributed to the ubiquitous carbon and is always observed on air exposed samples. The survey spectrum of the pure organic shell material, PTFS-GlcOH, shows C, O, F, and S as main components, but no Fe in accordance with its elemental composition. All the elements mentioned before can be detected in the sample of the coated particles, indicating that both components, magnetic nanoparticles as well as shell material, contribute to the spectrum. The comparison of all survey spectra reveals that the Fe and O peak intensities of PTFS-GlcOH-coated particles clearly decreased with respect to the pure nanoparticles, both in terms of absolute and relative intensity. The change of the relative C, F, O, and S peak intensities of the coated particles is much less pronounced compared to the spectrum of the pure shell material. Therefore, detected elements, relative peak intensities, and different peak shapes in the elemental region spectra imply that the magnetic nanoparticles are covered by the shell polymer. Particularly the background shape adjacent to the Fe2p emissions (Figure 5B) observed for the coated particles suggests the presence of magnetic nanoparticles enclosed by polymeric material rather than a mixture of both components. The Fe2p spectra show the typical structure for iron oxides with a broad, main, doublet peak ($Fe2p_{3/2}$ and $Fe2p_{1/2}$) and typical shakeup satellites, particularly well visible in the spectrum of the pure magnetic nanoparticles. The electron binding energy of the

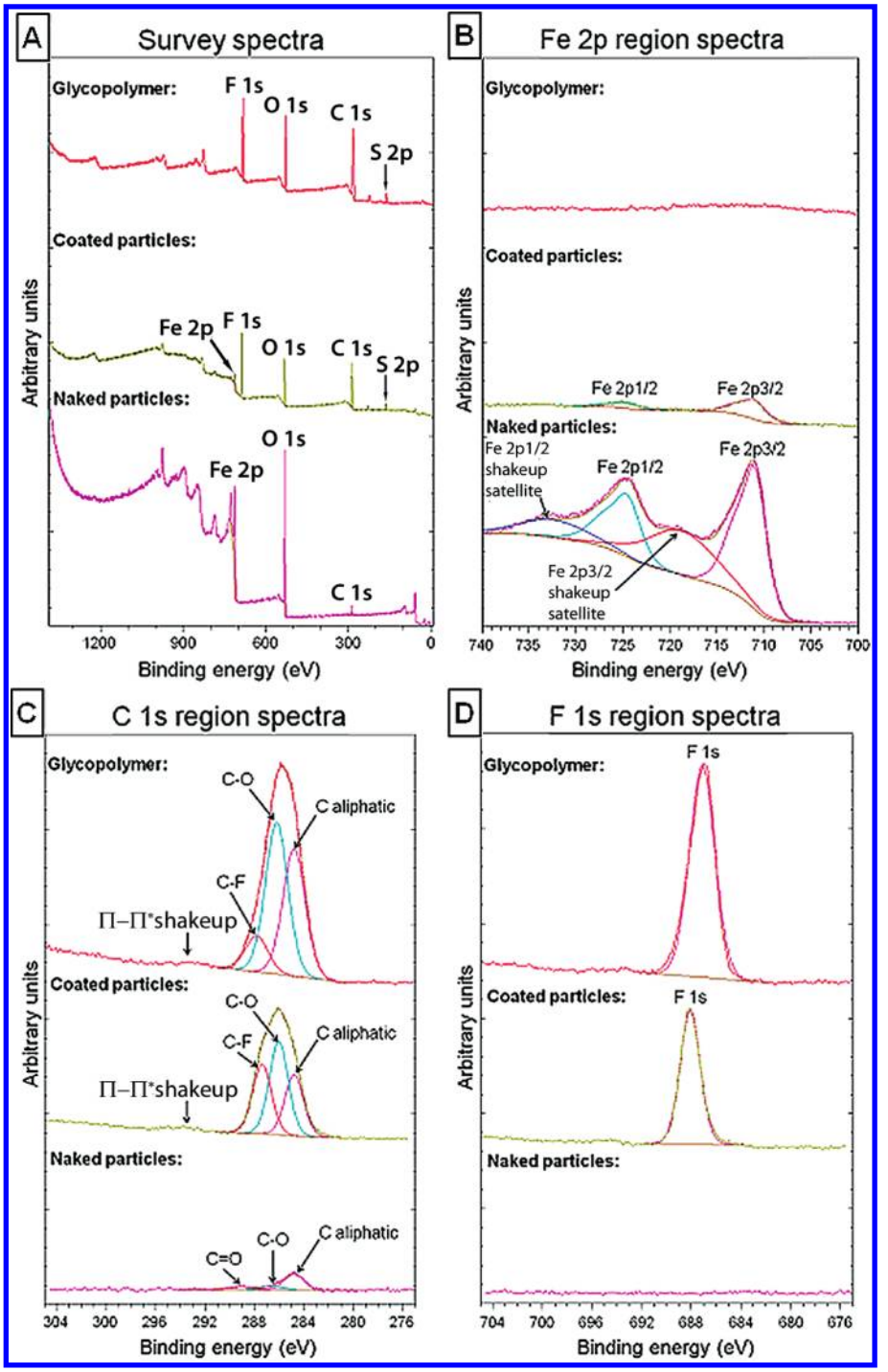

Figure 5. Selected XPS spectra of the synthesized glycopolymer, coated, and naked particles.

$Fe2p_{3/2}$ peak maximum of 711.1 eV and the peak shape, lacking the distinctive low-binding energy (BE) shoulder observed for Fe_3O_4, clearly point to Fe(III), thus, Fe_2O_3.[68] Furthermore, the Fe2p spectra, missing the high-BE shoulder reported for α-Fe_2O_3 (hematite), suggest that the outer part of the nanoparticles consist of γ-Fe_2O_3 (maghemite). This can be explained by gradual oxidation of the initially formed Fe(II) moieties to Fe(III). Hence, the spectra reveal the aging of the inorganic nanoparticle surface. The Fe2p spectral features of the coated particles are attenuated due to the coating of the particles by the polymeric material suggesting a shell thickness of slightly below 10 nm. The almost constant $Fe2p_{3/2}$ BE provides no indication for a strong chemical interaction between particle and shell that would result in a change of the chemical state. The C1s spectrum (Figure 5C) of pure magnetic nanoparticles is typical for minor surfaces contaminations always present on air-exposed surfaces. The three discrete states of carbon can be attributed to aliphatic C, functional groups with C−O single bonds, and to C═O double bonds.[69] The C1s spectrum region of the polymer component is marked by a clear increase of the peak intensity.

dx.doi.org/10.1021/bm101325w |*Biomacromolecules* 2011, 12, 681–691

Table 2. Data of XPS Analysis of the Glycopolymer, the Naked, and the Coated Nanoparticles

	C1s						O1s				F1s		S2p3/2		Fe2p3/2	
	C-aliphatic		C−O		C−F		FeO_x:		-OH							
region	%	eV	%	eV	%	eV	%	eV	%	eV	%	eV	%	eV	%	eV
naked	5.7	284.8	1.2	286.5	1.2	289.1	48.8	530.4	9.6	531.7	0.0		0.0		33.5	711.0
polymer	23.8	284.8	28.4	286.2	6.8	287.8	0.0		20.2	532.2	16.2	687.1	4.7	163.5	0.0	
coated	15.7	284.8	24.1	286.0	18.0	287.4	7.6	530.6	16.2	533.0	13.2	688.1	3.5	163.9	1.8	711.1

Also, the intensity distribution for the different chemical states is significantly altered. It is characterized by an increase of the C−O intensity becoming the most populous state. It can be attributed to the hydroxyl groups present in the carbohydrate units. Furthermore, another state appears in the C1s region of the glycopolymer belonging to the C−F bond of the poly(tetrafluorostyryl) groups. Since the spectrum envelope exhibits only little structure, it was decided to evaluate the lowest possible number of fitted states, which are at least indicated by the shape of the emission peak. The small increase of the background intensity on the high-BE side of the C1s peak system at about 293 eV is attributed to shakeup satellites indicating the π−system present in the polymer's aromatic rings.[70] The C1s spectrum of the coated particles shows a similar shape, however, the relative intensity of the C−F signal is increased markedly. This could point to a different orientation or configuration of the polymeric chains in the shell of the encased nanoparticles compared to the pure glycopolymer, possibly indicating that the F-containing units are oriented to the outer sphere of the shell and that the other polymeric units provide the interaction with the inorganic iron oxide core. The O1s spectrum (Supporting Information) of the inorganic nanoparticles is characterized by an asymmetric peak that can be separated into two components by fit. The main component, state 1, is attributed to O in Fe_2O_3; the minor component, state 2 on the high-BE side, to hydroxyl groups on the surface. The presence of the shell polymer encapsulating the nanoparticles leads in the O1s spectrum to a decrease of state 1 and an increase of the relative intensity and the BE of state 2, resembling the symmetric O1s emission of the pure organic shell material. The F1s BE in the spectrum of the coated particles (Figure 5D) is typical for F in organic polymers, with an exact value depending on the degree of fluorination.[70] The BE is higher than for the pure polymeric material as it is observed for the respective O1s, state 2, and S2p BEs, most likely due to an artifact introduced by assigning the C1s low-BE component to 284.8 eV. The S2p peak is only found in the spectra of the coated particles and the pure glycopolymer (Supporting Information). The BEs clearly indicate an organosulfidic -S- bond, which is assumed to facilitate the interaction between the nanoparticles core and the polymeric shell.[69]

vi. Thermogravimetric Analysis of the Glycopolymer-Coated Nanoparticles. The obtained particle suspensions as well as the polymeric shell material were dried under vacuum, and their thermal decomposition behavior was analyzed. The resulting thermogravimetric curves are presented in Figure 6.

The analysis of uncoated particles shows a total weight loss of 8% up to 900 °C. This behavior can be attributed to the remaining organic impurities and evaporation of water. The trace of the thermal decomposition of PTFS-GlcOH has two clear inflection points: one at 230 °C and a second at 429 °C, corresponding to the degradation of the glucose moieties and the tetrafluorostyryl backbone, respectively. The analysis curve of the coated particles shows the same decomposition temperatures as the glycopolymer, thus, proving the presence of the PTFS-GlcOH in the analyzed sample. From the remaining, nondegraded masses it can be calculated that the analyzed weight percent ratio between iron oxide and the coating material is approximately 1:5. This result is in good correlation with the XPS investigations, where the particle shell thickness was measured to be 10 nm.

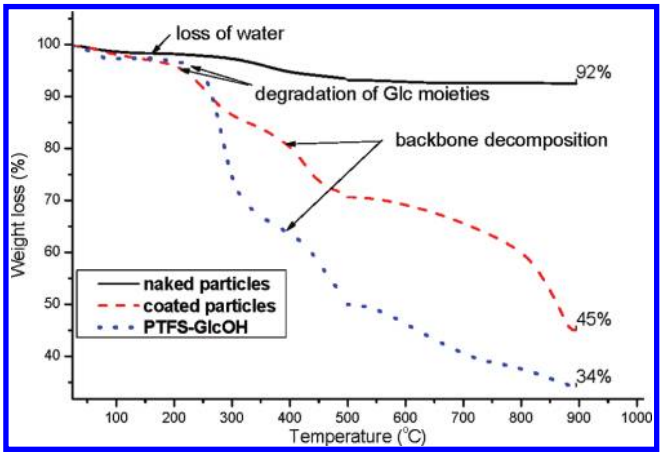

Figure 6. Traces from the thermogravimetric analysis of the prepared materials.

vii. Flow Cytometry Analyses of the Superparamagnetic Nanoparticles. Flow cytometry represents a powerful tool to characterize and analyze particles. It provides information about their size and shape from the forward and the side scattered light as well as about the fluorescence of particles in the analyzed sample.[71] The naked and coated particles were resuspended by sonication for 1 min at 10% amplitude, 30 min before analyses. Subsequently, 50 μL of the ferrofluid was diluted in 2 mL of Dulbecco's modified Eagle medium (DMEM) and vigorously agitated for 1 min. Afterward, the sample was directly analyzed by flow cytometry. The results can be found in Figure 7 (for the forward and side scattering plots, see the Supporting Information).

From the forward scattering traces, the size distribution of the analyzed particles can be estimated. The naked nanoparticles show a large size distribution of different agglomerates. The size distribution of the coated particles is much narrower, therefore, the polymer acts as the stabilizer, preventing agglomeration. Because the glycopolymer applied in the coating procedure was fluorescently labeled, the nanoparticles also show fluorescence thus proving the presence of the polymeric shell. To examine the stability of the ferrofluid, the coated particles were analyzed after 6 months storage at 8 °C. After resuspension, the flow cytometry analysis gave the same particle size distribution as for the freshly prepared nanoparticles (Supporting Information).

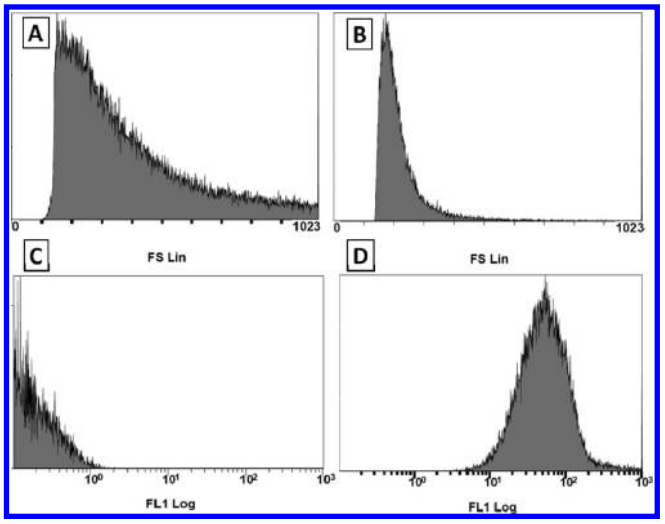

Figure 7. Results of flow cytometry analysis of the naked (A, C) and FITC-labeled, glycopolymer-coated particles (B, D): forward scattering (A, B); fluorescence (C, D).

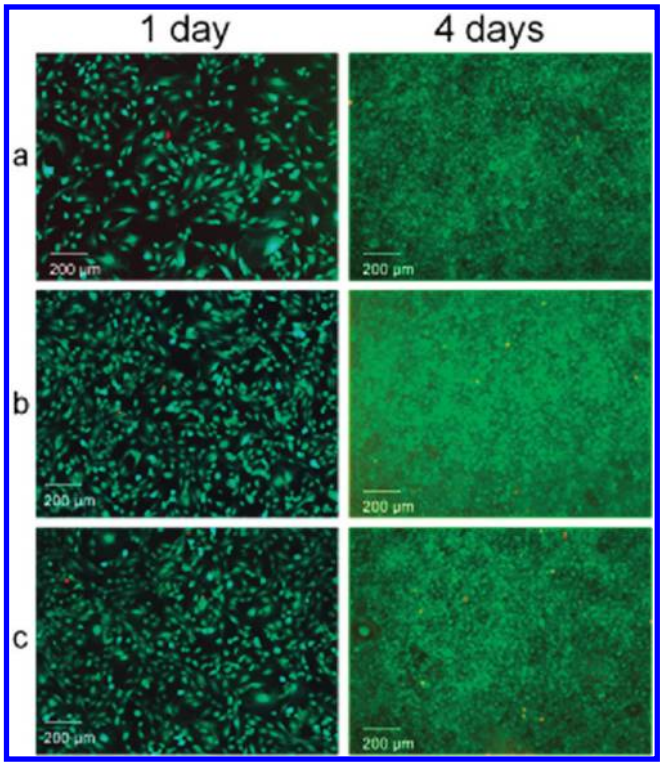

Figure 8. Fluorescence microscopy micrographs of FDA/EtBr stained 3T3 cells cultured for 1 day and 4 days in the presence of the glycopolymer-coated particles (obtained by image overlay of separately captured red and green fluorescence images). Top: control culture without particles, middle: 1% (v/v) particle suspension added, bottom: 5% (v/v) particle suspension added.

Investigation of Cytotoxicity. Exclusion of any cytotoxic effects is a primary prerequisite for the application of the obtained glycopolymer-coated particles in biology and medicine. Even if the targeted cells are planned to be eliminated, for example, tumor cells, no negative influence to the surrounding cells has to be ensured. Therefore, the cytotoxicity of the obtained particles toward 3T3 mouse fibroblasts was examined in a live/dead assay, using fluorescein diacetate (labeling living cells) and ethidium bromide (labeling the nuclei of dead cells). As shown in Figure 8, the addition of increasing amounts of the glycopolymer-coated nanoparticles, from 0.2% (not shown since uniform to control) to 1.0 and 5.0% (v/v), to the 3T3 fibroblast cells that were cultured for 4 days did not elevate the percentage of dead cells, only rarely observable as orange-stained nuclei, in comparison to a standard cell culture.

The number of dead cells was below 5% indicating no cytotoxic effects. The examined cells were adherent and showed a normal cell morphology. The increase in the cell number from about 20000−30000 cells·cm^{-2} after 1 day to about 170000−200000 cells·cm^{-2} after 4 days occurred independently from the amount of nanoparticles. Because no remarkable increase in cell number occurred during the first 24 h after cell seeding and the differences in adhesion are compensated after 4 h, the slightly lower cell density of the control, visible in Figure 8a, should result from random variations of the seeding procedure. This underlines that cell proliferation was not influenced by the presence of the particles. Furthermore, the absence of contaminations, for example, toxic residues of not converted reactants, catalysts, or solvents from the synthesis and preparation techniques was verified.

CONCLUSIONS

In summary, these results clearly demonstrate the applicability of glycopolymers based on poly(pentafluorostyrene) as stabilizing coating material of magnetic iron oxide nanoparticles. The synthesis of the new core−shell nanoparticles was performed in aqueous solution leading to stable ferrofluids. The polymeric shell was investigated in detail by XPS measurements displaying characteristic signals of the elements in the shell, and the magnetic nanoparticles exhibited the expected superparamagnetic behavior. Furthermore, flow cytometry measurements proved the stability of the obtained ferrofluids and the fluorescence of the nanoparticles. Investigations of the glycopolymer and the magnetic core−shell nanoparticles did not show any cytotoxic effects, emphasizing their applicability in biology and medicine. The double-labeled (magnetically and fluorescently) particles can be used for visualization of cell−carbohydrate interactions and magnetic separation investigations. In addition, the presented synthetic approach opens up a new, facile route for production of well-defined, glycopolymer-based materials of high purity and in large quantities. Further modifications of pentafluorostyryl monomers with various thiosugars and their polymerizations as well as copolymerizations are currently under investigation in our laboratories to introduce various thiosaccharide moieties into polymeric coatings of magnetic nanoparticles.

ASSOCIATED CONTENT

Supporting Information. ^{13}C NMR and HSQC-DEPT spectra (300 MHz, DMF-d_7) of the synthesized monomers and the glycopolymer. O1s and S2p region XPS spectra of the analyzed materials. Forward and side scattering plots of the flow cytometry analysis of FITC-labeled, PTFS-GlcOH-coated particles. Flow cytometry analysis results of the FITC-PTFS-GlcOH-coated particles after a 6-month storage. This material is available free of charge via the Internet at http://pubs.acs.org.

AUTHOR INFORMATION

Corresponding Author
*E-mail: ulrich.schubert@uni-jena.de.

ACKNOWLEDGMENT

We thank the Dutch Polymer Institute (DPI, Technologic Area HTE) and the German Federal Ministry of Economics and Technology (Contract Number VF080018) for financial support.

REFERENCES

(1) Winter, P. M.; Caruthers, S. D.; Kassner, A.; Harris, T. D.; Chinen, L. K.; Allen, J. S.; Lacy, E. K.; Zhang, H.; Robertson, J. D.; Wickline, S. A.; Lanza, G. M. *Cancer Res.* **2003**, *63*, 5838–5843.
(2) Wotschadlo, J.; Liebert, T.; Heinze, T.; Wagner, K.; Schnabelrauch, M.; Dutz, S.; Müller, R.; Steiniger, F.; Schwalbe, M.; Kroll, T. C.; Höffken, K.; Buske, N.; Clement, J. H. *J. Magn. Magn. Mater.* **2009**, *321*, 1469–1473.
(3) Alexiou, C.; Jurgons, R.; Schmid, R. J.; Bergemann, C.; Henke, J.; Erhard, W.; Huenges, E.; Parak, F. *J. Drug Targeting* **2003**, *11*, 139–149.
(4) Hergt, R.; Hiergeist, R.; Hilger, I.; Kaiser, W. A.; Lapatnikov, Y.; Margel, S.; Richter, U. *J. Magn. Magn. Mater.* **2004**, *270*, 345–357.
(5) Mykhaylyk, O.; Antequera, Y. S.; Vlaskou, D.; Plank, C. *Nat. Protoc.* **2007**, *2*, 2391–2411.
(6) Purushotham, S.; Ramanujan, R. V. *Acta Biomater.* **2010**, *6*, 502–510.
(7) Sosnovik, D. E.; Nahrendorf, M.; Weissleder, R. *Basic Res. Cardiol.* **2008**, *103*, 122–130.
(8) Shingel, K. I.; Marchessault, R. H. Iron-polysaccharide composites for pharmaceutical applications. In *Polysaccharides for Drug Delivery and Pharmaceutical Applications*; Marchessault, R. H., Ravenelle, F., Zhu, X. X., Eds.; American Chemical Society: Washington, DC, 2006; Vol. 934, pp 271−287.
(9) Earhart, C.; Jana, N. R.; Erathodiyil, N.; Ying, J. Y. *Langmuir* **2008**, *24*, 6215–6219.
(10) Purushotham, S.; Ramanujan, R. V. *J. Appl. Phys.* **2010**, *107*, 9.
(11) Li, G. L.; Zeng, D. L. M.; Wang, L.; Zong, B. Y.; Neoh, K. G.; Kang, E. T. *Macromolecules* **2009**, *42*, 8561–8565.
(12) Mykhaylyk, O.; Steingotter, A.; Perea, H.; Aigner, J.; Botnar, R.; Plank, C. *J. Biomed. Nanotechnol.* **2009**, *5*, 692–706.
(13) Sun, X. X.; Yang, G. L.; Sun, S. S.; Quan, R.; Dai, W. W.; Li, B.; Chen, C.; Li, Z. *Curr. Pharm. Biotechnol.* **2009**, *10*, 753–760.
(14) Pera, N. P.; Kouki, A.; Haataja, S.; Branderhorst, H. M.; Liskamp, R. M. J.; Visser, G. M.; Finne, J.; Pieters, R. J. *Org. Biomol. Chem.* **2010**, *8*, 2425–9.
(15) Wang, X.; Lin, J. M.; Ying, X. T. *Anal. Chim. Acta* **2007**, *598*, 261–267.
(16) Harrington, P. R.; Vinje, J.; Moe, C. L.; Baric, R. S. *J. Virol.* **2004**, *78*, 3035–3045.
(17) Behrens, S.; Bönnemann, H.; Matoussevitch, N.; Dinjus, E.; Modrow, H.; Palina, N.; Frerichs, M.; Kempter, V.; Maus-Friedrichs, W.; Heinemann, A.; Kammel, M.; Wiedenmann, A. *Z. Phys. Chem. (Muenchen, Ger.)* **2006**, *220*, 3–40.
(18) van Berkel, K. Y.; Piekarski, A. M.; Kierstead, P. H.; Pressly, E. D.; Ray, P. C.; Hawker, C. J. *Macromolecules* **2009**, *42*, 1425–1427.
(19) Pieters, R. J. *Med. Res. Rev.* **2007**, *27*, 796–816.
(20) Miura, Y. *J. Polym. Sci., Part A: Polym. Chem.* **2007**, *45*, 5031–5036.
(21) Coullerez, G.; Seeberger, P. H.; Textor, M. *Macromol. Biosci.* **2006**, *6*, 634–647.
(22) Ladmiral, V.; Melia, E.; Haddleton, D. M. *Eur. Polym. J.* **2004**, *40*, 431–449.
(23) Spain, S. G.; Cameron, N. R. *Polym. Chem.* **2010**, *2*, 60−68.
(24) Rye, P. D. *BioTechnology (Rajkot, India)* **1996**, *14*, 155–157.
(25) Rye, P. D.; Bovin, N. V. *Glycobiology* **1997**, *7*, 179–182.
(26) Sun, X. L.; Cui, W. X.; Haller, C.; Chaikof, E. L. *ChemBioChem* **2004**, *5*, 1593–1596.
(27) Yoo, M. K.; Kim, I. Y.; Kim, E. M.; Jeong, H. J.; Lee, C. M.; Jeong, Y. Y.; Akaike, T.; Cho, C. S. *J. Biomed. Biotechnol.* **2007**, Article ID 94740, 9 pages.
(28) Becer, C. R.; Babiuch, K.; Pilz, D.; Hornig, S.; Heinze, T.; Gottschaldt, M.; Schubert, U. S. *Macromolecules* **2009**, *42*, 2387–2394.
(29) Becer, C.; Hoogenboom, R.; Schubert, U. *Angew. Chem., Int. Ed.* **2009**, *48*, 4900–4908.
(30) Gottschaldt, M.; Koth, D.; Muller, D.; Klette, I.; Rau, S.; Goerls, H.; Schafer, B.; Baum, R. P.; Yano, S. *Chem. Eur. J.* **2007**, *13*, 10273–10280.
(31) Wagner, K.; Kautz, A.; Roeder, M.; Schwalbe, M.; Pachmann, K.; Clement, J. H.; Schnabelrauch, M. *Appl. Organomet. Chem.* **2004**, *18*, 514–519.
(32) Dreywood, R. *Ind. Eng. Chem., Anal. Ed.* **1946**, *18*, 499.
(33) Guiterrez Gallego, R.; Such-Sanmartin, G.; Segura, J. In *Recent Advances in Doping Analysis*; Schänzer, W., Geyer, H., Gotzmann, A., Mareck, U., Eds.; Sport und Buch Strauss: Köln, 2005; Vol. 13, p 383.
(34) Scott, T. A.; Melvin, E. H. *Anal. Chem.* **1953**, *25*, 1656–1661.
(35) Miyamoto, M.; Morimoto, Y.; Nozawa, Y.; Balamurugan, A. N.; Xu, B. Y.; Inoue, K. *Cell Transplant.* **2000**, *9*, 681–686.
(36) Brauer, D. S.; Russel, C.; Vogt, S.; Weisser, J.; Schnabelrauch, M. *J. Biomed. Mater. Res., Part A* **2007**, *80*, 410–420.
(37) Lindhorst, T. K. In *Topics in Current Chemistry*; Penadés, S., Ed.; Springer-Verlag: Berlin, Heidelberg, 2002; p 201.
(38) Spain, S. G.; Gibson, M. I.; Cameron, N. R. *J. Polym. Sci., Part A: Polym. Chem.* **2007**, *45*, 2059–2072.
(39) Wang, Q.; Dordick, J. S.; Linhardt, R. J. *Chem. Mater.* **2002**, *14*, 3232–3244.
(40) Ting, S. R. S.; Chen, G.; Stenzel, M. H. *Polym. Chem.* **2010**, *1*, 1392–1412.
(41) Okada, M. *Prog. Polym. Sci.* **2001**, *26*, 67–104.
(42) Voit, B.; Appelhans, D. *Macromol. Chem. Phys.* **2010**, *211*, 727–735.
(43) Slavin, S.; Burns, J.; Haddleton, D. M.; Becer, C. R. *Eur. Polym. J.* **2010**, DOI: 10.1016/j.eurpolymj.2010.09.019.
(44) Becer, C. R.; Schubert, U. S. *Adv. Polym. Sci.* **2010**, *225*, 17–62.
(45) Becer, C. R.; Kokado, K.; Weber, C.; Can, A.; Chujo, Y.; Schubert, U. S. *J. Polym. Sci., Part A: Polym. Chem.* **2010**, *48*, 1278–1286.
(46) Becer, C. R.; Paulus, R. M.; Hoogenboom, R.; Schubert, U. S. *J. Polym. Sci., Part A: Polym. Chem.* **2006**, *44*, 6202–6213.
(47) Ohno, K.; Fukuda, T.; Kitano, H. *Macromol. Chem. Phys.* **1998**, *199*, 2193–2197.
(48) Ohno, K.; Tsujii, Y.; Miyamoto, T.; Fukuda, T.; Goto, M.; Kobayashi, K.; Akaike, T. *Macromolecules* **1998**, *31*, 1064–1069.
(49) Ohno, K.; Izu, Y.; Yamamoto, S.; Miyamoto, T.; Fukuda, T. *Macromol. Chem. Phys.* **1999**, *200*, 1619–1625.
(50) Chen, Y.; Wulff, G. *Macromol. Chem. Phys.* **2001**, *202*, 3273–3278.
(51) Chen, Y.; Wulff, G. *Macromol. Chem. Phys.* **2001**, *202*, 3426–3431.
(52) Narumi, A.; Satoh, T.; Kaga, H.; Kakuchi, T. *Macromolecules* **2002**, *35*, 699–705.
(53) Narumi, A.; Matsuda, T.; Kaga, H.; Satoh, T.; Kakuchi, T. *Polymer* **2002**, *43*, 4835–4840.
(54) Miura, Y.; Koketsu, D.; Kobayashi, K. *Polym. Adv. Technol.* **2007**, *18*, 647–651.
(55) Ting, S. R. S.; Min, E. H.; Escale, P.; Save, M.; Billon, L.; Stenzel, M. H. *Macromolecules* **2009**, *42*, 9422–9434.
(56) Wulff, G.; Schmid, J.; Venhoff, T. *Macromol. Chem. Phys.* **1996**, *197*, 259–274.
(57) Samaroo, D.; Vinodu, M.; Chen, X.; Drain, C. M. *J. Comb. Chem.* **2007**, *9*, 998–1011.
(58) Pasetto, P.; Chen, X.; Drain, C. M.; Franck, R. W. *Chem. Commun.* **2001**, 81–82.
(59) Hoyle, C. E.; Lowe, A. B.; Bowman, C. N. *Chem. Soc. Rev.* **2010**, *39*, 1355–1387.

(60) Wilson, J. C.; Kiefel, M. J.; Angus, D. I.; von Itzstein, M. *Org. Lett.* **1999**, *1*, 443–446.
(61) Driguez, H. *ChemBioChem* **2001**, *2*, 311–318.
(62) Shen, H.; Byers, L. D. *Biochem. Biophys. Res. Commun.* **2007**, *362*, 717–720.
(63) Strähle, J.; Schweda, E. Jander/Blasius. *Einführung in das Anorganisch-Chemische Praktikum.*; S. Hirzel Verlag: Stuttgart-Leipzig, 1995; Vol. 14.
(64) Cao, H. N.; He, J.; Deng, L.; Gao, X. Q. *Appl. Surf. Sci.* **2009**, *255*, 7974–7980.
(65) Wagner, K.; Seemann, T.; Wyrwa, R.; Clement, J. H.; Müller, R.; Nietzsche, S.; Schnabelrauch, M. *Am. Inst. Phys. Conf. Proc.* **2010**, *1311*, 28–33.
(66) Gossuin, Y.; Gillis, P.; Hocq, A.; Vuong, Q. L.; Roch, A. *Wiley Interdiscip. Rev.-Nanomed. Nanobiotechnol.* **2009**, *1*, 299–310.
(67) Bulte, J. W. M.; Kraitchman, D. L. *NMR Biomed.* **2004**, *17*, 484–499.
(68) Grosvenor, A. P.; Kobe, B. A.; Biesinger, M. C.; McIntyre, N. S. *Surf. Interface Anal.* **2004**, *36*, 1564–1574.
(69) Briggs, D. *Surface Analysis of Polymers by XPS and Static SIMS*; Cambridge University Press: New York, 1998.
(70) Beamson, G.; Briggs, D. High Resolution XPS of Organic Polymers. *The Scienta ESCA300 Database*; John Wiley and Sons: New York, 1992.
(71) Siiman, O.; Jitianu, A.; Bele, M.; Grom, P.; Matijevic, E. *J. Colloid Interface Sci.* **2007**, *309*, 8–20.